HOKKAIDO UNIVERSITY

Title	Ligand-Assisted Back Energy Transfer in Luminescent Tb-III Complexes for Thermosensing Properties
Author(s)	Yamamoto, Masanori; Kitagawa, Yuichi; Nakanishi, Takayuki et al.
Citation	Chemistry-A European journal, 24(67), 17719-17726 https://doi.org/10.1002/chem.201804392
Issue Date	2018-12-03
Doc URL	https://hdl.handle.net/2115/76248
Rights	This is the peer-reviewed version of the following article: M. Yamamoto, Y. Kitagawa, T. Nakanishi, K. Fushimi, Y. Hasegawa, Chem. Eur. J. 2018, 24, 17719, which has been published in final form at http://doi.org/10.1002/chem.201804392. This article may be used for non-commercial purposes in accordance with Wiley-VCH Terms and Conditions for Self-Archiving.
Type	journal article
File Information	hase-Manuscript-final.pdf

Hokkaido University Collection of Scholarly and Academic Papers : HUSCAP

Ligand-assisted Back Energy Transfer in Luminescent Tb(III) Complexes for Thermo-sensing Properties

Masanori Yamamoto[a], Yuichi Kitagawa[b], Takayuki Nakanishi[c], Koji Fushimi[b], Yasuchika Hasegawa*[b]

Abstract: Luminescent Tb^{III} complex with hexafluoroacetylacetone (hfa) ligand shows a characteristic back energy transfer (BEnT), which leads to high temperature sensitivity for thermo-sensitive paint. Ligand-assisted BEnT by introducing of phosphine oxide into $Tb(hfa)_3$ complex defines as an effect of controlling activation energy (ΔE_a) and frequency factor (A) in BEnT process between Tb^{III} ion and hfa ligands. According to temperature-dependent emission lifetime measurements of mononuclear $Tb(hfa)_3$ complexes with monodentate phosphine oxides and polynuclear $Tb(hfa)_3$ complexes with bidentate phosphine oxides, the ΔE_a and A of polynuclear Tb^{III} complexes were smaller than those of mononuclear Tb^{III} complexes. Phosphorescence spectra and lifetimes of each $Gd(hfa)_3$ complex revealed that excited states of hfa ligands in Tb^{III}complex differs from polynuclear Tb^{III} complexes and mononuclear Tb^{III} complexes. The difference of ΔE_a and A value between polynuclear and mononuclear Tb^{III} complexes are caused by the formation of different excited states,such as delocalization of the excited state in the polynuclear Tb^{III} complexes and localization of excited states in the mononuclear Tb^{III} complexes. In particular, the small ΔE_a and small A values of polynuclear Tb^{III} complexes provide high effective activation of the BEnT under low temperature, resulting in high-sensitive temperature-dependent phosphor materials over wide range temperature.

Introduction

Thermosensitive paints containing luminescent materials enable temperature information about the substance surface to be obtained with high spatial resolution and a fast response.[1] Luminescent thermosensors are expected to be useful for capturing surface temperature dynamics of vehicles, aircrafts and chemical reactors.[2,3] The sensing mechanism is based on the temperature-depended luminescence intensities and lifetimes of organic compounds[4-6], metal complexes[7-9] and nanoparticles[10-12]. In particular, luminescent thermosensors containing lanthanide complexes have attracted attention for precise temperature imaging with narrow emission bands (full-width at half maximum (FWHM) < 10 nm) and long emission life-times (emission lifetime > 1 μs) based on the 4*f*-4*f* transitions.[13-16] In 2003, Amao and co-workers reported luminescent thermosensitive paint using the vibrational relaxation process of a red luminescent Eu^{III} complex.[14] In 2004, we described the temperature-sensing ability of a green luminescent Tb^{III} complex based on the back energy transfer (BEnT).[16] The energy transfer process from Tb^{III} to Eu^{III} in lanthanide coordination polymer has also been used for a ratiometric luminescent thermosensor.[17] The thermosensitive paints containing luminescent lanthanide complexes have also been widely investigated.[18-22]

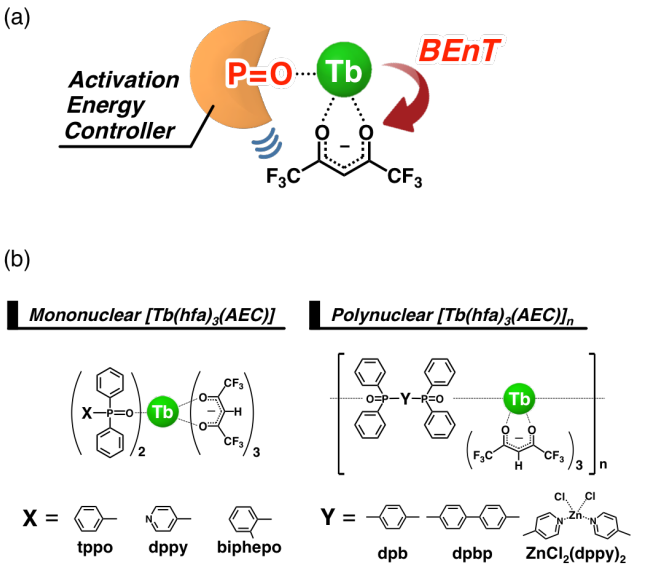

Figure 1. (a) Conceptual image of this study. (b) Chemical structure of $Tb(hfa)_3$(phosphine oxide) complexes.

Luminescent Tb^{III} complexes with BEnT are the most useful in molecular design unit for high-speed thermosensor. Here, we focus on the BEnT from excited state of Tb^{III} ($^5D_4$) to excited triplet state of the aromatic ligand (T_1) for thermosensing. The small energy gap between the $^5D_4$ and T_1 states (<1850 cm^{-1}) leads to effective BEnT in Tb^{III} complexes.[23] To control of the energy gap, pyridyl, diketonate and carbonyl ligands with aromatic derivatives in Tb^{III} complexes have been investigated.[24-28] Among these ligands, the hexafluoroacetylacetonate (hfa) ligand is one of the most promising candidates for development of thermosensitive luminescent Tb^{III} complexes (energy gap of hfa = 1700 cm^{-1}).[24,25] The hfa ligand also forms hydrogen bond networks in solid Tb^{III} complexes, which promotes the thermal stability in the high-temperature range.[29,30] The luminescent units composed of $Tb(hfa)_3$ complexes are suitable for thermosensitive paints based on the BEnT.

In general, the BEnT is depended on the activation energy (ΔE_a) and frequency factor (A) in the Arrhenius analysis.[27, 31]

[a] M. Yamamoto
Graduate School of Chemical Sciences and Engineering, Hokkaido University, North 13 West 8, Kita-ku, Sapporo, Hokkaido, 060-8628 (Japan).
[b] Dr. Y. Kitagawa, Dr. K. Fushimi, Prof. Dr. Y. Hasegawa
Faculty of Engineering, Hokkaido University, North 13 West 8, Kita-ku, Sapporo, Hokkaido, 060-8628 (Japan).
[c] Dr. T. Nakanishi
Faculty of Industrial Science and Technology, Tokyo University of Science, 6-3-1, Shinjuku, Katsushika-ku, Tokyo, 125-8585 (Japan).

Supporting information for this article is given via a link at the end of the document.((Please delete this text if not appropriate))

Controlling ΔE_a and A in $Tb(hfa)_3$ complexes improves the thermosensing ability for adjustable sensing range and temperature. In this study, activation energy control in BEnT of $Tb(hfa)_3$ complex is reported using activation energy controllers (AECs). The conceptual image of AECs is shown in Figure 1a. Here, we select the aromatic phosphine oxide ligand as an AEC molecule. The ΔE_a and A values of BEnT can be tuned by introducing the phosphine oxide ligand with a specific interaction with hfa ligand. The phosphine oxide ligand strongly coordinates to the lanthanide ion by P=O group.[32] The P=O group is also useful for enhancing the luminescence of lanthanide complexes based on suppression of nonradiative process via vibrational relaxation.[32] Luminescent Tb^{III} complexes with hfa and phosphine oxide ligands, mononuclear $[Tb(hfa)_3(AEC)]$ and polynuclear $[Tb(hfa)_3(AEC)]_n$: $[Tb(hfa)_3(tppo)_2]$, $[Tb(hfa)_3(biphepo)]$, $[Tb(hfa)_3(dppy)_2]$, $[Tb(hfa)_3(dpb)]_n$, $[Tb(hfa)_3(dpbp)]_n$ and $[Tb(hfa)_3ZnCl_2(dppy)_2]_n$ (tppo: trisphenylphosphine oxide, biphepo: [1,1'-biphenyl]-2,2'-diylbis(diphenylphosphine oxide), dppy: 4-pyridyldiphenylphosphine oxide, dpb: 1,4-phenylenebis(diphenylphosphine oxide), dpbp: [1,1'-biphenyl]-4,4'-diylbis(diphenylphosphine oxide)), were prepared for estimation of tunable ΔE_a and A values in their BEnT (Figure 1b). The emission properties of $[Tb(hfa)_3(AEC)]$ were evaluated using the emission spectra, emission lifetimes and emission quantum yields. To estimate the ΔE_a and A values in BEnT, Arrhenius analysis was performed using temperature-dependent emission lifetimes measurements. The triplet state lifetimes of hfa ligands were estimated using polynuclear and mononuclear Gd^{III} complexes. Introduction of phosphine oxide ligands to $Tb(hfa)_3$ complexes leads to control of the BEnT process, which is called ligand-assisted BEnT. This is the first report of control of thermosensing properties of the $Tb(hfa)_3$ complex by ligand-assisted BEnT.

Results and Discussion

Photophysical properties at room temperature

The mononuclear $[Tb(hfa)_3(AEC)]$ and polynuclear $[Tb(hfa)_3(AEC)]_n$ ($[Tb(hfa)_3(tppo)_2]$, $[Tb(hfa)_3(biphepo)]$, $[Tb(hfa)_3(dppy)_2]$, $[Tb(hfa)_3(dpb)]_n$, $[Tb(hfa)_3(dpbp)]_n$ and $[Tb(hfa)_3ZnCl_2(dppy)_2]_n$) were synthesized by reacting $[Tb(hfa)_3(H_2O)_2]$ precursor with phosphine oxide ligands in methanol under reflux. Single crystals of mononuclear $[Tb(hfa)_3(AEC)]$ and polynuclear $[Tb(hfa)_3(AEC)]_n$ were prepared by recrystallization from methanol solutions at room temperature (RT). The structural images and crystal data of $[Tb(hfa)_3(tppo)_2]$, $[Tb(hfa)_3(dpb)]_n$ and $[Tb(hfa)_3(dpbp)]_n$ are shown in Figure S1 and Table S1, respectively. From the single-crystal X-ray structural analysis results, the coordination sites of the Tb^{III} ion are comprised of three hfa and two phosphine oxide ligands (AEC ligands). Their coordination geometries based on the shape measure estimations are categorized as eight-coordinate square antiprism structures (see Figure S2 and Table S2-S4). The critical distance for dipole-dipole energy transfer between Tb^{III} ions was estimated to be approximately 5 Å (see supporting Information and Figure S8). In polynuclear $[Tb(hfa)_3(AEC)]_n$, the FRET-like energy transfer between Tb^{III} ions should not be inefficient. Single crystals of $[Tb(hfa)_3(biphepo)]$, $[Tb(hfa)_3(dppy)_2]$ and $[Tb(hfa)_3ZnCl_2(dppy)_2]_n$ were not obtained, and these structure could not be determined.

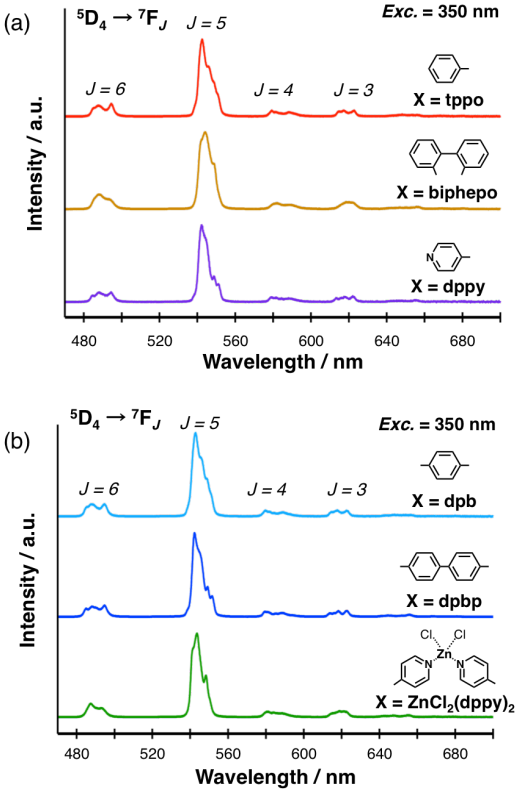

Figure 2. Emission spectra of (a) mononuclear $[Tb(hfa)_3(AEC)]$ and (b) polynuclear $[Tb(hfa)_3(AEC)]_n$ in the solid state at room temperature. Excited at 350 nm.

The emission spectra of the mononuclear $[Tb(hfa)_3(AEC)]$ and polynuclear $[Tb(hfa)_3(AEC)]_n$ complexes in solid state at RT are shown in Figure 2. Emission bands are observed at 487, 548, 582, and 623 nm, which are attributed to $4f$–$4f$ transitions of the Tb^{III} complexes ($^5D_4 \rightarrow {}^7F_J$, where J = 6, 5, 4, and 3, respectively). The Stark splitting shapes at 548nm ($^5D_4 \rightarrow {}^7F_5$) for mononuclear $[Tb(hfa)_3(AEC)]$ are similar to those for polynuclear $[Tb(hfa)_3(AEC)]_n$. In particular, the stark splitting shapes of $[Tb(hfa)_3(tppo)_2]$ and $[Tb(hfa)_3(dppy)_2]$ are much similar to those of $[Tb(hfa)_3(dpb)]_n$ and $[Tb(hfa)_3(dpbp)]_n$ (see Figure S9a). Generally, the Stark splitting shape of emission spectrum of a lanthanide complex is dependent on the coordination geometry. From Figure S9b, the coordinate structure of $[Tb(hfa)_3(dppy)_2]$ should also be eight-coordinate square antiprism structure, such as $[Tb(hfa)_3(dpbp)]_n$. We found that the emission spectral shape of $[Tb(hfa)_3(biphepo)]$ with eight-coordinate square antiprism structure is similar to that of $[Tb(hfa)_3ZnCl_2(dppy)_2]_n$.

The emission decay of mononuclear $[Tb(hfa)_3(AEC)]$ and polynuclear $[Tb(hfa)_3(AEC)]_n$ complexes in solid state at 300 K are shown in Figure S3. The emission lifetimes of the $[Tb(hfa)_3(AEC)]$ complexes (τ_{obs}) were determined from the slope of the logarithmic decay profiles. The emission decay of the

mononuclear $[Tb(hfa)_3(AEC)]$ and polynuclear $[Tb(hfa)_3(AEC)]_n$ complexes showed microsecond-scale emission lifetime by estimating single-exponential fitting. The overall emission quantum yields (Φ_{tot}) by excitation of the hfa ligands in solid state at RT were measured using the integration sphere. The photophysical parameters (Φ_{tot} and $\tau_{obs,\ RT}$) are summarized in Table 1. The Φ_{tot} values of $[Tb(hfa)_3(tppo)_2]$, $[Tb(hfa)_3(biphepo)]$ and $[Tb(hfa)_3(dppy)_2]$ are 9.2%, 11%, and 10%, respectively. In contrast, the Φ_{tot} values of $[Tb(hfa)_3(dpbp)]_n$ (17%) and $[Tb(hfa)_3ZnCl_2(dppy)_2]_n$ (35%) are significantly larger than those of mononuclear $[Tb(hfa)_3(AEC)]$ complexes, although the Φ_{tot} value of $[Tb(hfa)_3(dpb)]_n$ (10%) is similar to those of mononuclear $[Tb(hfa)_3(AEC)]$ complexes. These results indicate that the photosensitized emission quantum yields of polynuclear Tb^{III} complexes are dependent on the phosphine oxide linker moiety. We consider that introduction of phosphine oxide ligand affects the photosensitized energy transfer process between the hfa ligands and the Tb^{III} ion.

Temperature-dependent emission properties

To estimate the effect of BEnT in the mononuclear $[Tb(hfa)_3(AEC)]$ and polynuclear $[Tb(hfa)_3(AEC)]_n$ complexes, the temperature-dependent emission lifetimes in solid state were measured in the range 90–400 K. The logarithmic lifetime profiles of a typical Tb^{III} complex with the tppo ligand, $[Tb(hfa)_3(tppo)_2]$, are shown in Figure 3a. From Figure 3a, emission decay profiles from 100 K to 200 K were shown single-exponential decays, but emission decay profiles from 250 K to 400 K were shown multi-exponential decays. In higher temperature range, we consider that at least two types of emission species are coexisted in solid states. The emission decay of $[Tb(hfa)_3(tppo)_2]$ analyzed single-exponential decays at each temperature by treating emission lifetime as an average value. The emission lifetimes of the mononuclear $[Tb(hfa)_3(tppo)_2]$ complexes at 100 K, 200 K, 300 K, and 400K are 806 μs, 709 μs, 86 μs, and 5.6 μs, respectively. The longer emission lifetimes at 100-200 K are because of suppression of the BEnT process from emitting level of the Tb^{III} ion ($^5D_4$) to the triplet state of the hfa ligands (T_1). The temperature-dependent emission lifetimes are observed for all of the mononuclear $[Tb(hfa)_3(AEC)]$ and polynuclear $[Tb(hfa)_3(AEC)]_n$ complexes. （see Figure S4 and S5）.

To analyze the BEnT mechanism, we estimated the BEnT rate constants (k_{BEnT}) by kinetic analysis. The temperature dependence of k_{BEnT} is expected to follow an Arrhenius-type equation with an activation energy ΔE_a. [17] k_{BEnT} is given by

$$\ln\left(\frac{1}{\tau_{obs}}-\frac{1}{\tau_{90K}}\right)=\ln k_{BEnT}=\ln A-\frac{\Delta E_a}{R}\cdot T^{-1} \qquad (1),$$

where τ_{obs}, τ_{90K}, A, ΔE_a, R and T are the observed emission lifetime, standard emission lifetime at 90 K, frequency factor, activation energy, gas constant and temperature, respectively. Arrhenius plots of BEnT for the mononuclear $[Tb(hfa)_3(AEC)]$ and polynuclear $[Tb(hfa)_3(AEC)]_n$ complexes are shown in Figure 3b, and the ΔE_a and A values are given in Table 1. The BEnT process diagram is shown in Figure S6. From Figure 3b,

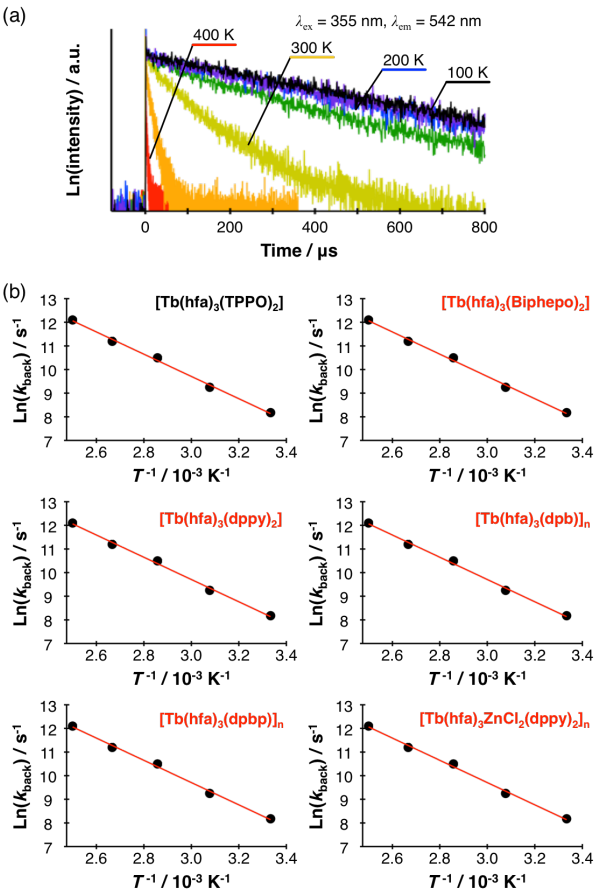

Figure 3. (a) Temperature-dependent emission lifetime decays of $[Tb(hfa)_3(tppo)_2]$ in the solid state among 100-400 K. Excited at 355 nm (third harmonics of Q-switched Nd:YAG laser. fwhm =5 ns, λ = 1064 nm, black line: 100 K, purple line: 150 K, blue line: 200 K, green line: 250 K, yellow line: 300K, orange line: 350 K, red line 400 K). (b) Arrhenius plots of each each $Tb(hfa)_3$ complex in the solid state.

Table 1. Photophysical properties and Arrhenius parameters of [Tb(hfa)(AEC)]

	Conformation	Φ_{tot}	$\tau_{obs,\ RT}$	ΔE_a	A
		%	μs	cm^{-1}	s^{-1}
$[Tb(hfa)_3(tppo)_2]$	Mononuclear	9.2±1	209±3	3200	1.98×10^{10}
$[Tb(hfa)_3(biphepo)]$	Mononuclear	11±1	267±12	4000	3.56×10^{11}
$[Tb(hfa)_3(dppy)_2]$	Mononuclear	10±1	482±9	3600	1.06×10^{10}
$[Tb(hfa)_3(dpb)]_n$	Polymer	9.7±1	73±5	1700	4.06×10^{7}
$[Tb(hfa)_3(dpbp)]_n$	Polymer	17±2	215±4	1900	3.68×10^{7}
$[Tb(hfa)_3ZnCl_2(dppy)_2]_n$	Polymer	35±2	610±7	2500	7.92×10^{7}

the Arrhenius plot of mononuclear $[Tb(hfa)_3(AEC)]$ and polynuclear $[Tb(hfa)_3(AEC)]_n$ could be analyzed by linear approximation. These results indicate that the BEnT process is only composed of between Tb^{III} ions and hfa ligands. The ΔE_a

values of polynuclear $[Tb(hfa)_3(AEC)]_n$ complexes ($[Tb(hfa)_3(dpb)]_n$, $[Tb(hfa)_3(dpbp)]_n$ and $[Tb(hfa)_3ZnCl_2(dppy)]_n$) are smaller than those of mononuclear $[Tb(hfa)_3(AEC)]$ complexes ($[Tb(hfa)_3(tppo)_2]$, $[Tb(hfa)_3(biphepo)]$ and $[Tb(hfa)_3(dppy)_2]$). The A values of polynuclear $[Tb(hfa)_3(AEC)]_n$ are also smaller than those of mononuclear $[Tb(hfa)_3(AEC)]$.

According to the polynuclear Tb^{III} complexes, the ΔE_a value of $[Tb(hfa)_3(dpb)]_n$ (ΔE_a = 1700 cm^{-1}) and $[Tb(hfa)_3(dpbp)]_n$ (ΔE_a = 1900 cm^{-1}) are smaller than those of $[Tb(hfa)_3ZnCl_2(dppy)]_n$ (ΔE_a = 2500 cm^{-1}). The A value of $[Tb(hfa)_3(dpb)]_n$ (A = 4.06×10^7 s^{-1}) and $[Tb(hfa)_3(dpbp)]_n$ (A =73.68×10^7 s^{-1}) are also smaller than those of $[Tb(hfa)_3ZnCl_2(dppy)]_n$ (A = 7.92×10^7 s^{-1}).The smaller ΔE_a and A values of polynuclear $[Tb(hfa)_3(AEC)]_n$ complex promote effective activation of BEnT under lower temperature, resulting in high-sensitive temperature-dependent phosphor materials over a wide range temperature. The phosphine oxide ligand (activation energy controller: AEC) should dominate not only the Tb^{III} molecular structures (mononuclear or polymer) but also the BEnT process (ΔE_a and A values).

Phosphorescence properties of mononuclear $[Gd(hfa)_3(AEC)]$ and polynuclear $[Gd(hfa)_3(AEC)]_n$

The calculated ΔE_a and A values of mononuclear $[Tb(hfa)_3(AEC)]$ and polynuclear $[Tb(hfa)_3(AEC)]_n$ complexes are directly linked to the triplet levels of hfa ligands in the $Tb(hfa)_3$ complexes. In this study, to estimate the triplet levels of the hfa ligands, mononuclear $[Gd(hfa)_3(AEC)]$ and polynuclear $[Gd(hfa)_3(AEC)]_n$ complexes ($[Gd(hfa)_3(tppo)_2]$, $[Gd(hfa)_3(biphepo)]$, $[Gd(hfa)_3(dppy)_2]$, $[Gd(hfa)_3(dpb)]_n$, $[Gd(hfa)_3(dpbp)]_n$ and $[Gd(hfa)_3ZnCl_2(dppy)]_n$) were prepared by the same synthetic method as that used to prepare the mononuclear $[Tb(hfa)_3(AEC)]$ and polynuclear $[Tb(hfa)_3(AEC)]_n$ complexes. Generally, the triplet state properties of photosensitized ligands in lanthanide complexes can be evaluated by phosphorescence measurements of the Gd^{III} complexes, because the excited energy level of the Gd^{III} ion is higher than the T_1 level of photosensitized hfa ligand. We confirmed that phosphine oxide ligands were not excited at 350 or 355 nm based on diffuse reflection spectra of Gd^{III} complexes and phosphine oxide ligand (see Figure S11). The phosphorescence spectra of the mononuclear $[Gd(hfa)_3(AEC)]$ and polynuclear $[Gd(hfa)_3(AEC)]_n$ complexes in solid states at 100 K are shown in Figure 4. The phosphorescence spectrum shapes of the polynuclear $[Gd(hfa)_3(dpb)]_n$ and $[Gd(hfa)_3(dpbp)]_n$ complexes are broader than those of the mononuclear $[Gd(hfa)_3(AEC)]$ and polynuclear $[Gd(hfa)_3ZnCl_2(dppy)_2]_n$ complexes. These results indicate that the vibrational structure of the excited hfa ligand in the polynuclear $[Gd(hfa)_3(dpb)]_n$ and $[Gd(hfa)_3(dpbp)]_n$ complexes are considerably different from those of the mononuclear $[Gd(hfa)_3(AEC)]$ and polynuclear $[Gd(hfa)_3ZnCl_2(dppy)_2]_n$ complexes. The broader phosphorescence bands of $[Gd(hfa)_3(dpb)]_n$ and $[Gd(hfa)_3(dpbp)]_n$ could be caused by the change of the potential curvature of the triplet state in the excited hfa ligands. From the phosphorescence spectra, the estimated triplet energy levels of the hfa ligands in the Gd^{III} complexes $E(T_1)$ are summarized in

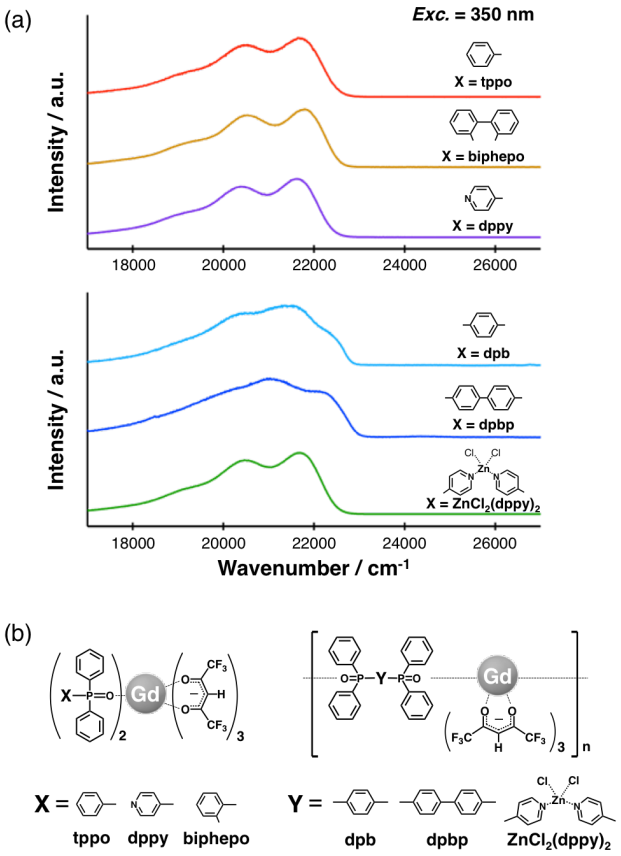

Figure 4. (a) Phosphorescence spectra of mononuclear $[Gd(hfa)_3(AEC)]$ and polynuclear $[Gd(hfa)_3(AEC)]_n$ in the solid state at 100 K. Excited at 350 nm (Time delay = 0 ms). (b) Chemical structure of $Gd(hfa)_3$(phosphine oxide) complexes.

Table 2. Triplet energies and phosphorescence lifetimes of hfa ligands

	Conformation	$E(T_1)$	$\Delta E(T_1\text{-}^5D_4)$	$\tau_{obs,1}$	$\tau_{obs,2}$
		cm^{-1}	cm^{-1}	ms	ms
$[Gd(hfa)_3(tppo)_2]$	Mononuclear	21700	1300	2.00 (70%)	9.12 (30%)
$[Gd(hfa)_3(biphepo)]$	Mononuclear	21800	1400	2.94 (68%)	9.41 (32%)
$[Gd(hfa)_3(dppy)_2]$	Mononuclear	21600	1200	1.96 (71%)	8.25 (29%)
$[Gd(hfa)_3(dpb)]_n$	Polymer	22400	2000	3.31 (79%)	9.54 (21%)
$[Gd(hfa)_3(dpbp)]_n$	Polymer	22300	1900	3.30 (80%)	10.2 (20%)
$[Gd(hfa)_3ZnCl_2(dppy)_2]_n$	Polymer	21700	1300	2.02 (65%)	7.75 (35%)

Table 2. We also give the energy gap $\Delta E(T_1\text{-}^5D_4)$ between the triplet level of the hfa ligands (T_1) and emitting level of Tb (energy gap of $^5D_4$ = 20400 cm^{-1}). The $\Delta E(T_1\text{-}^5D_4)$ values of the polynuclear Tb^{III} complexes $[Tb(hfa)_3(dpb)]_n$ and

$[Tb(hfa)_3(dpbp)]_n$ were larger than those of mononuclear $[Tb(hfa)_3(AEC)]$ complexes, although the ΔE_a values of the BEnT process for $[Tb(hfa)_3(dpb)]_n$ and $[Tb(hfa)_3(dpbp)]_n$ are smaller than those of mononuclear $[Tb(hfa)_3(AEC)]$ complexes. From these photophysical conflicts, we propose that the BEnT process is related to the triplet states lifetimes of hfa ligands in our systems.

Here, the phosphorescence decay measurements were performed to estimation of the triplet state lifetimes on the excited hfa ligands. The logarithmic lifetime profiles of the Gd^{III} complexes are shown in Figure S7, and the calculated phosphorescence lifetimes are summarized in Table 2. The phosphorescence decay exhibited double exponential decay at 100 K. Note that the $Tb(hfa)_3$ units is composed of three identical hfa ligands from single-crystal X-ray structural analyses. The double exponential decay of hfa phosphorescence is caused by the presence of at least two types of excited hfa ligands in the solid state. The phosphorescence lifetimes of the polynuclear $[Gd(hfa)_3(dpb)]_n$ and $[Gd(hfa)_3(dpbp)]_n$ complexes are longer than those of the mononuclear $[Gd(hfa)_3(AEC)]$ and polynuclear $[Gd(hfa)_3ZnCl_2(dppy)_2]_n$ complexes.

Here, we here consider that the polynuclear $[Gd(hfa)_3(dpb)]_n$ and $[Gd(hfa)_3(dpbp)]_n$ complexes promote energy transfer hopping (migration) of excited Tb^{III} ions on the dpb and dpbp linker ligands, [33] resulting in delocalization of the excited triplet state of hfa ligand. This excited delocalization is related to the broader phosphorescence spectra and long phosphorescence lifetimes of the hfa ligands, which promotes ligand-assisted BEnT. The excited states of mononuclear $[Tb(hfa)_3(AECs)]$ complexes with large ΔE_a and large A values only depend on localization between Tb^{III} and hfa ligands in the

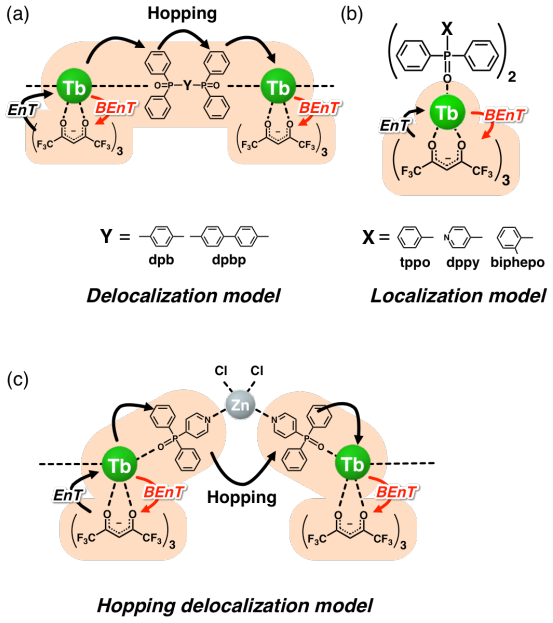

Figure 5. (a) Excited energy delocalization image of polynuclear $[Tb(hfa)_3(dpb)]_n$ and $[Tb(hfa)_3(dpbp)]_n$. (b) Excited energy localization image of mononuclear $[Tb(hfa)_3(AEC)]$. (c) Excited energy delocalization image of polynuclear $[Tb(hfa)_3ZnCl_2(dppy)_2]$.

forward and back energy transfer process, resulting in short phosphorescence lifetime and large frequency factor A (Figure 5b). For the polynuclear $[Tb(hfa)_3ZnCl_2(dppy)_2]_n$ complex, the ΔE_a and A values are similar to those of the polynuclear $[Tb(hfa)_3(dpb)]_n$ and $[Tb(hfa)_3(dpbp)]_n$ complexes. However, the phosphorescence spectrum shape of the polynuclear $[Gd(hfa)_3ZnCl_2(dppy)_2]_n$ complex is the same as that of mononuclear $[Gd(hfa)_3(dppy)_2]$ complex. From these results, we consider that $[Tb(hfa)_3ZnCl_2(dppy)_2]_n$ shows localized forward and back energy transfer between the hfa and Tb^{III} ions (short phosphorescent lifetimes and phosphorescent spectrum shapes), and delocalized energy hopping of excited Tb^{III} ions via the phosphine oxide linker ligands (show small ΔE_a and small A) (Figure 5c).

Conclusions

Introduction of phosphine oxide ligands (Activation Energy Controllers: AECs) to $Tb(hfa)_3$ complexes leads to control of the BEnT process (the ligand-assisted BEnT). From Arrhenius analysis based on the temperature-dependent emission lifetime measurements, the ΔE_a and A values are smaller for the polynuclear $[Tb(hfa)_3(AEC)]_n$ complexes than for the mononuclear $[Tb(hfa)_3(AEC)]$ complexes. In particular, $[Tb(hfa)_3ZnCl_2(dppy)_2]_n$ shows a wider sensing range and larger emission quantum yields than the previous reported chameleon luminophore structure $[Tb_{0.99}Eu_{0.01}(hfa)_3(dpbp)]_n$.[17,33] The phosphorescent lifetimes of the hfa ligands in the Gd^{III} coordination polymers are longer than those in mononuclear $[Gd(hfa)_3(AEC)]$ complexes. We consider that the energy hopping of excited Tb^{III} ions and hfa ligands is introduced by the phosphine oxide linker ligand in polynuclear $[Gd(hfa)_3(AEC)]_n$ complexes. The ΔE_a and A values in the BEnT process are a strongly correlated with the excitation lifetimes of the hfa ligands. Introduction of phosphine oxide ligands to $Tb(hfa)_3$ complexes is expected to control the BEnT process. This is the first report of the thermosensing properties of the $Tb(hfa)_3$ complex by ligand-assisted BEnT.

Experimental Section

Materials: Terbium acetate tetrahydrate (>99.9%), *n*-BuLi (in *n*-hexane, 1.6 M) and hydrogen peroxide were purchased from Kanto Chemical Co., Inc. Hexafluoroacetylacetone (>95.0%), triphenylphosphine oxide (>98.0%), 2,2'-bis(diphenylphosphino)biphenyl (>98.0%), 1,4-dibromobenzene (>99.0%), 4,4'-dibromobiphenyl (>98.0%) and chlorodiphenylphosphine (>97.0%) were obtained from Tokyo Chemical Industry Co., Ltd. All other chemicals and solvents were reagent grade and were used without further purification.

Apparatus: ^1H NMR spectra were recorded using a JEOL JNM-ECS400 (400 MHz). ^1H NMR chemical shifts were determined by tetramethylsilane (TMS) as an internal standard. Infrared spectra were recorded using a JASCO FT/IR-4600. Elemental analyses were performed using an Exeter Analytical, Inc. CE-440 Elemental Analyzer.

Preparation of [1,1'-biphenyl]-2,2'-diylbis(diphenylphosphine oxide) (biphepo) $C_{36}H_{28}O_2P_2$: Biphepo was obtained by the same method as previously reported by Nakamura et al.[34] 2,2'-Bis(diphenylphosphino)biphenyl (500 mg, 1.60 mmol) added into 20 ml of dichloromethane, and cooled under 0˚C and then 30% H_2O_2 aqueous solution (30%) was add to the solution. The reaction mixture was stirred for 3 h. After the reaction, the product was extracted with dichloromethane (30 ml × 3), and then washed with brine for three times. The dichloromethane solution was dried using anhydrous $MgSO_4$ and concentrated to dryness. The biphepo was recovered as a white solid. Yield: 336 mg (38%). ^{1}H NMR (400 MHz, $CDCl_3$ / TMS): δ7.73-7.69(t, 4H), 7.66-7.63(t, 4H), 7.53-7.50(t, 2H), 7.47-7.43(t, 4H), 7.36-7.33(t, 2H), 7.31-7.28(t, 4H), 7.20-7.15(m, 6H), 7.00(t, 2H)ppm. IR (ART): 1210 (st, P=O) cm^{-1}.

Preparation of 4-pyridyl diphenyl phosphine oxide (dppy) $C_{17}H_{14}NOP$: Dppy was prepared according to literature references.[35] ^{1}H NMR (400MHz, $CDCl_3$/TMS): δ8.74-8.79 (t, 2H, py), 7.48-7.71 (m, 12H, Ar) ppm. ESI-MS calcd. for $[M+H]^+$: 280.09 Found, 280.09. Elemental analysis calcd (%) for $C_{17}H_{14}NOP$: C 73.11, H 5.05, N 5.02; found: C 73.03, H, 5.07; N, 4.95.

Preparation of 1,4-phenylenebis(diphenylphosphine oxide) (dpb) $C_{30}H_{24}O_2P_2$: 1,4-phenylenebis(diphenylphosphine oxide) was synthesized according to the published procedure.[36] A solution of *n*-BuLi (12.5 mL, 1.6 M, 20 mmol), was added dropwise to a solution of 1,4-dibromobenzene (2.36 g, 10 mmol) in dry THF (30 mL) at –80˚C. The addition was completed in ca. 15 min during which time a yellow precipitate was formed. The mixture was allowed to stir for 3 h at –10˚C, after which a chlorodiphenylphosphine (2.7 mL, 20 mmol) was added dropwise at –80˚C. The mixture was gradually brought to room temperature, and stirred for 14 h. The product was extracted with dichloromethane, the extracts washed with brine for three times and dried over anhydrous $MgSO_4$. The obtained white solid and dichloromethane (ca. 40 mL) were placed in a flask. The solution was cooled to 0˚C and then 30% H_2O_2 aqueous solution (5 mL) was added to it. The reaction mixture was stirred for 2 h. The product was extracted with dichloromethane, the extracts washed with brine for three times and dried over anhydrous $MgSO_4$. The solvent was evaporated, and resulting residue was washed with ethyl acetate for several times, and filtered in vacuum to afford a white powder. Yield: 2.5 g (52%). ^{1}H NMR (400 MHz, $CDCl_3$ / TMS): δ7.48-7.78 (m, 24H, *p*-C_6H_5, C_6H_4) ppm. IR (ART): 1121 (st, P=O) cm^{-1}.

Preparation of [1,1'-biphenyl]-4,4'-diylbis(diphenylphosphine oxide) (dpbp) $C_{36}H_{28}O_2P_2$: 4,4'-bis(diphenylphosphoryl)biphenyl was synthesized according to the published procedure. [36] A solution of *n*-BuLi (9.3 mL, 1.6 M hexane, 15 mmol), was added dropwise to a solution of 4,4'-dibromobiphenyl (1.9 g, 6.0 mmol) in dry THF (30 mL) at –80˚C. The addition was completed in ca. 15 min during which time a yellow precipitate was formed. The mixture was allowed to stir for 3 h at –10˚C, after which a chlorodiphenylphosphine (2.7 mL, 15 mmol) was added dropwise at –80˚C. The mixture was gradually brought to room temperature, and stirred for 14 h. The product was extracted with dichloromethane, the extracts washed with brine for three times and dried over anhydrous $MgSO_4$. The obtained white solid and dichloromethane (ca. 40 mL) were placed in a flask. The solution was cooled to 0˚C and then 30% H_2O_2 aqueous solution (5 mL) was added to it. The reaction mixture was stirred for 2 h. The product was extracted with dichloromethane, the extracts washed with brine for three times and dried over anhydrous $MgSO_4$. The solvent was evaporated, and resulting residue was washed with ethyl acetate for several times, and filtered in vacuum to afford a white powder. Yield: 1.1 g (33%). ^{1}H NMR (400 MHz, $CDCl_3$ / TMS): δ7.67-7.80 (m, 16H, *p*-C_6H_5, C_6H_4), 7.45-7.60 (m, 12H, *p*-C_6H_5, C_6H_4) ppm. IR (ART): 1120 (st, P=O) cm^{-1}.

Preparation of $[ZnCl_2(dppy)_2]$ $C_{34}H_{28}Cl_2N_2O_2P_2Zn$. $[ZnCl_2(dppy)_2]$ was prepared according to literature references.[35] ^{1}H NMR (400MHz, $CDCl_3$/TMS): δ8.84-8.89 (t, 4H, py), 7.71-7.77 (d, 4H, py), 7.62-7.70 (m, 12H, Ar), 7.50-7.57 (m, 8H, Ar) ppm. ESI-MS calcd. for $[ZnCl(dppy)_2]^+$: 692.03 Found, 692.03. Elemental analysis calcd (%) for $C_{34}H_{28}Cl_2N_2O_2P_2Zn$: C 58.77, H 4.06, N 4.03; found: C 59.27, H 4.31, N 3.73.

Preparation of $[Tb(hfa)_3(H_2O)_2]$ $C_{15}H_7F_{18}O_8Tb$: $[Tb(hfa)_3(H_2O)_2]$ was prepared according to literature reference.[16] Terbium acetate tetrahydrate (2.4 g, 5.9 mmol) was dissolved in distilled water (30 mL). Hexafluoroacetylacetone (4.0 g, 19 mmol) was added dropwise to the solution and let stirred for 3 h at room temperature to form pale yellow precipitates. The reaction mixture was filtered and washed with distilled water. The resulting powder was used without further purification for the next step. Yield 4.1 g (85%). IR (ART): 1647 (st, C=O), 1251, 1204,1135 (st, C-F) cm^{-1}. Elemental analysis calcd (%) for $C_{15}H_7F_{18}O_8Tb$: C 22.08, H 0.86; found: C 21.68, H 1.14.

Preparation of $[Tb(hfa)_3(tppo)_2]$ $C_{51}H_{33}F_{18}O_8P_2Tb$: Methanol (50mL) containing $[Tb(hfa)_3(H_2O)_2]$ (294 mg, 0.36 mmol) and triphenylphosphine oxide: tppo (200 mg, 0.72 mmol) was fluxed under stirring for 3 h. The reaction mixture was concentrated with evaporator. Recrystallization from methanol gave colorless crude crystals. Yield: 150 mg (31%). IR (ART): 1653 (st, C=O), 1250,1140 (st, C-F), 1161, 1122 (st, P=O) cm^{-1}. Elemental analysis calcd (%) for $C_{51}H_{33}F_{18}O_8P_2Tb$: C 45.83, H 2.49; found: C 45.19, H 2.49.

Preparation of $[Tb(hfa)_3(biphepo)]$ $C_{51}H_{31}F_{18}O_8P_2Tb$: Methanol (100 mL) containing $[Tb(hfa)_3(H_2O)_2]$ (294 mg, 0.36 mmol) and biphepo (200 mg, 0.36 mmol) was refluxed under stirring for 3 h. The reaction mixture was concentrated with evaporator. Recrystallization from methanol gave white crystal. Yield: 176 mg (36%). IR (ART): 1654 (st, C=O), 1253, 1140 (st, C-F), 1180, 1124 (st, P=O) cm^{-1}. Elemental analysis calcd (%) for $C_{51}H_{31}F_{18}O_8P_2Tb$: C 45.90, H 2.34; found: C 45.53, H 2.43.

Preparation of $[Tb(hfa)_3(dppy)_2]$ $C_{49}H_{31}F_{18}N_2O_8P_2Tb$: Methanol (50mL) containing $[Tb(hfa)_3(H_2O)_2]$ (294 mg, 0.36 mmol) and dppy (200 mg, 0.72 mmol) was fluxed under stirring for 3 h. The reaction mixture was concentrated with evaporator. Recrystallization from methanol gave colorless crude crystals. Yield: 110 mg (23%). IR (ART): 1652 (st, C=O), 1251, 1140 (st, C-F), 1170-1108 (st, P=O) cm^{-1}. Elemental analysis calcd (%) for $C_{49}H_{31}F_{18}N_2O_8P_2Tb$: C 43.97, H 2.33, N 2.09; found: C 44.19, H 2.45, N 1.87.

Preparation of $[Tb(hfa)_3(dpb)]_n$ $C_{45}H_{27}F_{18}O_8P_2Tb$: $[Tb(hfa)_3(H_2O)_2]$ (343 mg, 0.42 mmol) and dpb (200 mg, 0.42 mmol) were dissolved in methanol (15 mL). The solution was refluxed while stirring for 3 h to give a white precipitate. The precipitate was filtered, washed with methanol for several times, and dried in vacuum. Yield: 213 mg (40%). IR (ART): 1652 (st, C=O), 1252, 1138 (st, C-F), 1186-1106 (st, P=O) cm^{-1}. Elemental analysis calcd (%) for $C_{45}H_{27}F_{18}O_8P_2Tb$: C 42.95, H 2.16; found: C 43.28, H 2.04.

Preparation of $[Tb(hfa)_3(dpbp)]_n$ $C_{51}H_{31}F_{18}O_8P_2Tb$: $[Tb(hfa)_3(H_2O)_2]$ (294 mg, 0.36 mmol) and dpbp (200 mg, 0.36 mmol) were dissolved in methanol (15 mL). The solution was refluxed while stirring for 3 h to give a white precipitate. The precipitate was filtered, washed with methanol for several times, and dried in vacuum. Yield: 184 mg (38%). IR (ART): 1652 (st, C=O), 1250, 1139 (st, C-F), 1182, 1123 (st, P=O) cm^{-1}. Elemental

analysis calcd (%) for $C_{51}H_{31}F_{18}O_8P_2Tb$: C 45.90, H 2.34; found: C 45.65, H 2.19.

Preparation of $[Tb(hfa)_3ZnCl_2(dppy)_2]_n$ $C_{49}H_{31}Cl_2F_{18}N_2O_8P_2TbZn$: $[Tb(hfa)_3(H_2O)_2]$ (237 mg, 0.29 mmol) and $[ZnCl_2(dppy)_2]$ (200 mg, 0.29 mmol) were dissolved in methanol (15 mL). The solution was refluxed while stirring for 3 h to give a white precipitate. The precipitate was filtered, washed with methanol for several times, and dried in vacuum. Yield: 123 mg (29%). IR (ART): 1649 (st, C=O), 1253, 1181-1132 (st, C-F), 1217-1106 (st, P=O) cm^{-1}. Elemental analysis calcd (%) for $C_{49}H_{31}Cl_2F_{18}N_2O_8P_2TbZn$: C 39.90, H 2.12, N 1.90; found: C 39.56, H 2.35, N 1.86.

Preparation of mononuclear $[Gd(hfa)_3(AEC)]$ and polynuclear $[Gd(hfa)_3(AEC)]_n$: Mononuclear $[Gd(hfa)_3(AEC)]$ and polynuclear $[Gd(hfa)_3(AEC)]_n$ were prepared by the same synthetic method as that used to prepare the mononuclear $[Tb(hfa)_3(AEC)]$ and polynuclear $[Tb(hfa)_3(AEC)]_n$ complexes.

$[Gd(hfa)_3(tppo)_2]$ $C_{51}H_{33}F_{18}O_8P_2Gd$: IR (ART): 1652 (st, C=O), 1253,1140 (st, C-F), 1167, 1122 (st, P=O) cm^{-1}. Elemental analysis calcd (%) for $C_{51}H_{33}F_{18}O_8P_2Gd$: C 45.89, H 2.49; found: C 45.42, H 2.89.

$[Gd(hfa)_3(biphepo)]$ $C_{51}H_{31}F_{18}O_8P_2Gd$: IR (ART): 1654 (st, C=O), 1250, 1139 (st, C-F), 1181, 1124 (st, P=O) cm^{-1}. Elemental analysis calcd (%) for $C_{51}H_{31}F_{18}O_8P_2Gd$: C 45.90, H 2.34; found: C 46.23, H 2.45.

$[Gd(hfa)_3(dppy)_2]$ $C_{49}H_{31}F_{18}N_2O_8P_2Gd$: IR (ART): 1652 (st, C=O), 1251, 1140 (st, C-F), 1170-1108 (st, P=O) cm^{-1}. Elemental analysis calcd (%) for $C_{49}H_{31}F_{18}N_2O_8P_2Gd$: C 44.02, H 2.34, N 2.10; found: C 44.46, H 2.47, N 2.19.

$[Gd(hfa)_3(dpb)]_n$ $C_{45}H_{27}F_{18}O_8P_2Gd$: IR (ART): 1653 (st, C=O), 1252, 1138 (st, C-F), 1190-1106 (st, P=O) cm^{-1}. Elemental analysis calcd (%) for $C_{45}H_{27}F_{18}O_8P_2Gd$: C 43.00, H 2.17; found: C 43.29, H 1.92.

$[Gd(hfa)_3(dpbp)]_n$ $C_{51}H_{31}F_{18}O_8P_2Gd$: IR (ART): 1652 (st, C=O), 1250, 1139 (st, C-F), 1180, 1123 (st, P=O) cm^{-1}. Elemental analysis calcd (%) for $C_{51}H_{31}F_{18}O_8P_2Gd$: C 45.95, H 2.34; found: C 45.65, H 2.19.

$[Gd(hfa)_3ZnCl_2(dppy)_2]_n$ $C_{49}H_{31}Cl_2F_{18}N_2O_8P_2GdZn$: IR (ART): 1650 (st, C=O), 1181-1132 (st, C-F), 1215-1105 (st, P=O) cm^{-1}. Elemental analysis calcd (%) for $C_{49}H_{31}Cl_2F_{18}N_2O_8P_2GdZn$: C 39.95, H 2.12, N 1.90; found: C 39.75, H 2.22, N 1.95.

Crystallography: Colorless single crystals of $Tb(hfa)_3$ complexes were mounted on the MiTeGen micromesh using paraffin oil. All measurements were made by using a Rigaku RAXIS RAPID imaging-plate area detector with graphite-monochromated Mo-Kα radiation. Non-hydrogen atoms were refined anisotropically. All calculations were performed by using the crystal-structure crystallographic software package. CIF data was confirmed by using the checkCIF/PLATON service. CCDC-1862802 {for $[Tb(hfa)_3(TPPO)_2]$} , -1862803 {for $[Tb(hfa)_3(dpb)]_n$}and -1862804 {for $[Tb(hfa)_3(dpbp)]_n$} contain the supplementary crystallographic data for this paper. These data can be obtained free of charge from The Cambridge Crystallographic Data Centre via www.ccdc.cam.ac.uk/data_request/cif.

Optical measurements: UV−Vis absorption spectra were recorded on a JASCO V-670 spectrometer. Emission and excitation spectra of $Tb(hfa)_3$ complexes were measured with a HORIBA Fluorolog-3 spectrofluorometer and corrected for the response of the detector system.The wavelength resolution of Fluorolog-3 found to be 0.05 nm. The error of the phosphorescence spectra at 430 nm (phosphorescence edge of Gd^{III} complexes) was estimated to be 5 cm^{-1}. Emission lifetimes (τ_{obs}) of coordination polymers were measured using the third harmonics (355 nm) of a Q-switched Nd:YAG laser (Spectra Physics, INDI-50, FWHM = 5 ns, λ = 1064 nm) and a photomultiplier (Hamamatsu photonics, R5108, response time ≤ 1.1 ns). The Nd:YAG laser response was monitored with a digital oscilloscope (Sony Tektronix, TDS3052, 500 MHz) synchronized to the single-pulse excitation. Emission lifetimes were determined from the slope of logarithmic plots of the decay profiles. Emission lifetimes in the range 100–400 K were measured using a cryostat (Thermal Block Company, SA-SB245T) and a temperature controller (Oxford, Instruments, ITC 502S). We carried out all photophysical measurements of Tb^{III} and Gd^{III} complexes with cut filter under 385 nm (LU0385 longpass filter, Asahi Spectra Co., Ltd.).The emission quantum yields excited at 350 nm (Φ_{tot}) were estimated using a JASCO F-6300-H spectrometer attached with JASCO ILF-533 integrating sphere unit (φ = 100 nm). The wavelength dependence of the detector response and the beam intensity of the Xe light source for each spectrum were calibrated using a standard light source.

Computational Details: Density functional theory (DFT) geometry optimizations of $[ZnCl_2(dppy)_2]$ and Time-dependent DFT (TD-DFT) of phosphine oxide ligands were carried out with Gaussian09 Rev D.01 by employing the three-parameter hybrid functional of Becke based on the correlation functional of Lee, Yang, and Parr (B3LYP).[37,38] The 6-31G*(d, P) basis set was used for all other atoms.

Acknowledgements

This work was supported by JSPS KAKENHI (grant number 18H04497). This work was also partially supported by a Grant-in-Aid for Scientific Research on the 18H02041 from the Ministry of Education, Culture, Sports, Science and Technology (MEXT), Japan. This present research was supported by the Ministry of Education, Culture, Sports, Science and Technology through Program for Leading Graduate Schools (Hokkaido University “Ambitious Leader’s Program”). We thank Edanz Group (www.edanzediting.com/ac) for editing a draft of this manuscript.

Keywords: Thermosensitive paint・Lanthanide complex・Back energy transfer・Luminescence

[1] X.-D. Wang, O. S. Wolfbeis, R. J. Meier, *Chem. Soc. Rev*., **2013**, *42*, 7834-7869.
[2] S. Clauchety, H. Sakaue, *Sens. Actuator, B-Chem*., **2017**, *251*, 958-962.
[3] V. Ondrus, R. J. Meier, C. Klein, U. Henne, M. Schäferling, U. Beifuss, *Sens. Actuator, A-Phys*., **2015**, *233*, 434-441.
[4] D. Ross, M. Gaitan, L. E. Locascio, *Anal. Chem*., **2001**, *73*, 4117–4123.
[5] X. Guan and Z. Su, *Polym. Adv. Technol*., **2008**, *19*, 385–392.
[6] J. Feng, K. Tian, D. Hu, S. Wang, S. Li, Y. Zeng, Y. Li, G. Yang, *Angew. Chem. Int. Ed*., **2011**, *50*, 8072–8076.
[7] K. Maruszewski, D. Andrzejewski, W. Strek, *J. Lumin*., **1997**, *72–74*, 226–228.
[8] L. H. Fischer, C. Karakus, R. J. Meier, N. Risch, O. S. Wolfbeis, E. Holder, M. Schäferling, *Chem. Eur. J*., **2012**, *18*, 15706–15713.
[9] J. Stehr, J. M. Lupton, M. Reufer, G. Raschke, T. A. Klar, J. Feldmann, *Adv. Mater*., **2004**, *16*, 2170–2174.

[10] V. A. Vlaskin, N. Janssen, J. van Rijssel, R. m. Beaulac, D. R. Gamelin, *Nano Lett.*, **2010**, *10*, 3670–3674.

[11] R. Liang, R. Tian, W. Shi, Z. Liu, D. Yan, M. Wei, D. G. Evans, X. Duan, *Chem. Commun.*, **2013**, *49*, 969–971.

[12] A. Sedlmeier, D. E. Achatz, L. H. Fischer, H. H. Gorris, O. S. Wolfbeis, *Nanoscale*, **2012**, *4*, 7090–7096.

[13] J. -C. G. Bünzli, *Chem. Rev*., **2010**, *110*, 2729-2755.

[14] M. Mittsuishi, S. Kikuchi, T. Miyashita, Y. Amao, *J. Mater. Chem.*, **2003**, *13*, 2875–2879.

[15] J. H. S. K. Monteiro, F. A. Sigoli, A. de Battencourt-Dias, *Can. J. Chem.*, **2017**, 1–6.

[16] S. Katagiri, Y. Hasegawa, Y. Wada, S. Yanagida, *Chem. Lett.*, **2004**, *33*, 1438–1439.

[17] K. Miyata, Y. Konno, T. Nakanishi, A. Kobayashi, M. Kato, K. Fushimi, Y. Hasegawa, *Angew. Chem. Int. Ed.*, **2013**, *52*, 6413-6416.

[18] X. Liu, S. Akerboom, M. de jong, I. Mutikainen, S. Tanase, A. Meijerink, E. Bouwman, *Inorg. Chem.*, **2015**, *54*, 11323–11329.

[19] Z. Wang, D. Ananias, A. Carné-Sánchez, C. D. S. Brites, I. Imaz, D. Maspoch, J. Rocha,; L. D. Carlos, *Adv. Funct. Mater.*, **2015**, *25*, 2824–2830.

[20] Y. Cui, H. Xu, Y. Yue, Z. Guo, Z. Chen, J. Gao, Y. Yang, G. Qian, B. Chen, *J. Am. Chem. Soc.*, **2012**, *134*, 3979–3982.

[21] K. Yanagisawa, Y. Kitagawa, T. Nakanishi, T. Seki, K. Fushimi, H. Ito, Y. Hasegawa, *Chem. Eur. J.*, **2018**, *24*, 1956–1961.

[22] C. D. S. Brites, P. P. Lima, N. J. O. Silva, A. Millan, V. S. Amaral, F. Palacio, L. D. Carlos, *Adv. Mater.* **2010**, *22*, 4499–4504.

[23] M. Latva, H. Takalo, V.-M. Mukkala, C. Matachescu, J. C. Rodriguez-Ubis, J. Kankare, *J. Lumin.*, **1997**, *75*, 149-169.

[24] V. I. Tasryuk, A. V. Vologzhanina, K. P. Zhuravlev, V. A Kudryshova, *J. Fluorine. Chem.*, **2017**, *197*, 87–93.

[25] S. Katagiri, Y. Tsukahara, Y. Hasegawa, Y. Wada, *Bull. Chem. Soc. Jpn.*, **2007**, *8*, 1492–1503.

[26] Q. Xu, Z. Li, Y. Wang, H. Li, *Photochem. Photobiol. Sci.*, **2016**, *15*, 405-411.

[27] S. Omagari, T. Nakanishi, T. Seki, Y. Kitagawa, Y. Takahata, K. Fushimi, H. Ito, Y. Hasegawa, *J. Phys. Chem. A.*, **2015**, *119*, 1943–1947.

[28] F. Gutrierrez, C. Tedeschi, L. Maron, J-.P. Daudey, R. Poteau, J. Azema, P. Tisnes, C. Picard, *Dalton Trans.*, **2004**, *0*, 1334–1347.

[29] Y. Hirai, T. Nakanishi, Y. Kitagawa, K. Fushimi, T. Seki, H. Ito, Y. Hasegawa, *Angew. Chem. Int. Ed.*, **2016**, *128*, 12238–12241.

[30] T. Koizuka, M. Yamamoto, Y. Kitagawa, T. Nakanishi, K. Fushimi, Y. Hasegawa, *Bull. Chem Soc. Jpn.,* **2017**, *90*, 1287–1292.

[31] S. Omagari, T. Nakanishi, T. Seki, Y. Kitagawa, T. Seki, K. Fushimi, H. Ito, A. Meijerink, Y. Hasegawa, *Sci. Rep.*, **2016**, *6*, 37008–37018.

[32] Y. Hasegawa, Y. Wada, S. Yanagida, *J. Photochem. Photobiol.C,* **2004**, *5*, 183–202.

[33] M. Hatanaka, Y. Hirai, Y. Kitagawa, T. Nakanishi, Y. Hasegawa, K. Morokuma, *Chem. Sci.*, **2017**, *8*, 423–429

[34] K. Nakamura, Y. Hasegawa, H. Kawai, N. Yasuda, N. Kanehisa, Y. Kai, T. Nagamura, S. Yanagida, Y. Wada, *J. Phys. Chem. A.*, **2007**, *111*, 3029–3037.

[35] M. Yamamoto, T. Nakanishi, Y. Kitagawa, K. Fushimi, Y. Hasegawa, *Mater. Lett.*, **2016**, *167*, 183–187.

[36] K. Miyata, T. Ohba, A. Kobayashi, M. Kato, T.Nakanishi, K. Fushimi, Y. Hasegawa, *ChemPlusChem*, **2012**, *77*, 277–280.

[37] C. Lee, W. Yang, R. G. Parr, *Phos. Rev. B*, **1988**, *37*, 785-789.

[38] A. D. Becke, *J. Chem. Phys*. **1993**, *98*, 5648-5652.

Entry for the Table of Contents

FULL PAPER

This study presents that the effect (Ligand-assisted BEnT) on the back energy transfer process between Tb ions and hfa (hexafluoroacetylacetone) ligands for the $Tb(hfa)_3$ complexes with introducing various phosphine oxide ligands (activation energy controllers: AECs) .

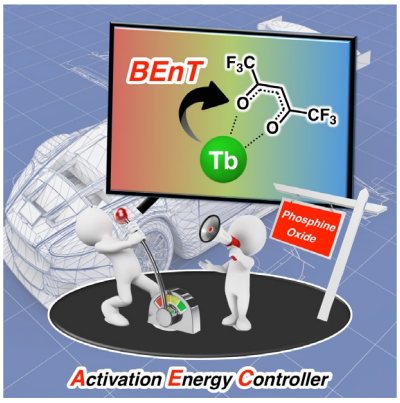

*Masanori Yamamoto, Yuichi Kitagawa, Takayuki Nakanishi, Koji Fushimi, Yasuchika Hasegawa**

Page No. – Page No.

Ligand-assisted back energy transfer in luminescent Tb(III) complexes for thermo-sensing properties